JOURNAL OF SOLID STATE CHEMISTRY 35, 391–401 (1980)

Microscopic Observations on the Thermal Decomposition of α-Aluminum Hydride*†

P. J. HERLEY,‡ O. CHRISTOFFERSON, AND J. A. TODD§

Department of Materials Science and Engineering, State University of New York, Stony Brook, New York 11794

Received December 17, 1979; in revised form March 24, 1980

The various isothermal and photolytic decomposition stages of α-aluminum hydride have been examined by scanning electron microscopy. The pristine material consists of cuboids, 50–100 μm on a side, some of which are contact or interpenetrating twins. The interpenetrating twin axis appears to be the [001] body diagonal of the cuboids. The cuboids' surface, which has been chemically treated to promote thermal stability, contains faceted pits whose sides lie along close-packed directions. The pit interiors show evidence of layering. During the thermal induction period, patches containing acicular filaments, each ~0.005 μm in diameter and ~0.3 μm in length, of Al-metal are formed and are dispersed randomly on the internal crystal surfaces. During the acceleratory period, a large number of additional patches appear in which some of the filaments cluster together to form small clumps. The acicular filaments in all patches thicken and increase slightly in length as the reaction proceeds. Later in the acceleratory period, bubbles (0.2 to 3.5 μm in diameter) appear. The bubbles are randomly distributed throughout the cuboid and produce isolated volumes (~2 to 7 μm in diameter) of partially reacted AlH_3. Eventually, the filaments spread over the entire internal substructure of the cuboid. However, although completely decomposed, the cuboid remains intact. Preexposure to 1.0×10^9 R ^{60}Co γ rays blackens the surface and produces a "rougher" external surface with some densely decomposed patches and many more filaments. Additional patches containing denser clusters of acicular nuclei were observed in the surface after uv photolysis at room temperature and at 150°C. At 150°C delamination of the surface layer occasionally occurs in the coirradiated material. The increased number of nuclei formed by preirradiation and uv photolysis confirm kinetic studies which postulate the presence of additional nuclei formed by the irradiation.

Introduction

This investigation on the effects observed microscopically during isothermal decomposition is directed toward understanding the chemical processes influencing the reactivity of α-aluminum hydride (AlH_3). α-AlH_3 is chemically stable at room temperature. However, some evidence is forthcoming that it ages slowly over a period of several years (*1*). The powder evolves hydrogen irreversibly without melting when isothermally decomposed *in vacuo* between 100 and 150°C (*2*). These decomposition kinetic studies suggest that the reaction

$$AlH_3(s) \rightarrow Al(s) + \tfrac{3}{2} H_2(g)$$

* Research supported by the U.S. Department of Energy under Contract E(11-1)-2715.

† Presented in part, at the International Symposium on the Properties and Applications of Metal Hydrides, Colorado Springs, Colorado, April 1980.

‡ To whom all correspondence should be addressed.

§ Present address: Department of Materials Science and Mineral Engineering, University of California, Berkeley, California 94720.

0022-4596/80/150391-11$02.00/0

develops by a process involving the formation, growth, and ingestion of heterogeneous nuclei (*1*). The location of the initial sites for decomposition often depends on solid-state defects on or just below the crystal surface (e.g., points where dislocations emerge on the surface (*3*)). This study attempts to identify the nature of the decomposition nucleus and whether the nuclei form at specific locations and grow along specific directions during decomposition.

In isothermal kinetic studies involving the evolution of hydrogen gas as a function of time the fractional decomposition $\alpha = p(t)/p_f$, where $p(t)$ is the pressure at time, t, and, p_f, the final pressure, can be related to a series of mathematical equations describing nucleation formation and growth (*4–6*). However, the application of a suitable equation and its degree of fit alone is insufficient to justify the assignment of a specific type of mechanism to the overall process unless supported by other, independent evidence, e.g., microscopy, electrical conductivity data, etc. The purpose of this report is to seek supportive evidence for the use of the specific kinetic equations that were found applicable to the thermal decomposition curves for α-AlH_3 (*1, 2*). These equations imply random nucleation proceeding from discrete nuclei (with or without slow growth) followed by nuclei overlap and the formation of a contiguous interfacial area which decreases over the decay stage.

To date, the only available report in the literature concerning microscopic evidence of the thermal decomposition is one on polycrystalline AlH_3 powder (*7*). The authors state that the thermal decomposition reaction nucleates predominantly at a face of the crystal and then the reaction front moves along the "*c*" axis direction. Examination of the crystal at various stages was not discussed and results were not presented on the nature of the nuclei, the reaction interface, or the effect of photolytic or radiation-induced decomposition.

Thus we have undertaken a detailed and systematic microscopic study of the events occurring during the isothermal decomposition of α-AlH_3 powder *in vacuo*. Also, the effects of γ-ray preirradiation on the subsequent thermal decomposition and the effects of photolytic decomposition at temperatures ranging from ambient to 150°C on the decomposition process were examined. Although the samples were examined optically in many instances, this report will emphasize particularly the scanning electron microscope evidence.

Experimental

Material

The α-AlH_3 powder used in this study was obtained from Dr. R. H. Wiswall, Jr. and J. J. Reilly, Department of Molecular Sciences, Brookhaven National Laboratory. This powder corresponds to α-AlH_3 (pattern 1451) manufactured by the Dow Chemical Company, Midland, Michigan. Details of the synthesis of this material are provided in Ref. (*11*). The powder has been characterized by Turley and Rinn (*8*). The material was found to crystallize in the trigonal space group $R\bar{3}c$, with six molecules in a hexagonal unit cell of dimensions $a = 4.449$ Å, $c = 11.804$ Å. X-Ray diffraction data obtained using an Enraf–Nonius CAD 4 diffractometer with CuK_α radiation confirmed the space group and unit cell dimensions of $a = 4.455(8)$ Å, $c = 11.83(1)$ Å were found using 16 reflections. X-Ray powder patterns using CuK_α, normalized to the peak of maximum intensity, show a 1 : 1 correspondence to those previously reported (*8*).

The powder consists of minute cuboids, light gray in color, with side lengths 50–100 μm (see Plate 1a). The material was stored in the dark over anhydrous calcium sulfate

prior to use. All handling procedures were carried out in dry air. The percentage purity of the material has been reported (*9*) to be 95–98 wt%. The percentage decomposition of a 60-mg sample decomposed to $\alpha = 1$ was found to be 97% as determined from weight-loss measurements using a Perkin–Elmer Am-1 autobalance. A mass spectrometric study of the gaseous products evolved under continuous heating indicated trace quantities of CO_2, H_2O, N_2, and O_2.

Apparatus

The specimens examined in this study were obtained after pretreatment in a high-vacuum Pyrex-glass photolysis apparatus similar in design to those reported earlier (*10*). The photolysis sample was confined to a sample container consisting of two 1-in. square fused silica flats, 2 mm thick, fused together along the edges. The top flat had a 1-cm-diameter hole drilled in the center of it to contain the sample. An ionization gauge was used to monitor the background pressures and pressures during pumpdown. The gas pressures evolved during the experiment were recorded in a 4-liter volume containing a liquid nitrogen trap on a Baratron differential micromanometer (MKS Instruments Type 77), with the reference side pumped continuously.

In addition to photolysis, the present system is capable of running simultaneous isothermal and photolysis decompositions above room temperature. This capability was accomplished by surrounding the entire reaction tube by a small furnace controlled to ±0.3°C.

Procedure

The tared samples for decomposition were placed directly onto the quartz sample holder and after insertion into the system, were pumped overnight (12–16 hr) with a background pressure ~1.2–4.0 × 10^{-7} Pa. The outgassing rate of the isolated sample/system was 0.0010 Pa/min. The specimen temperature never exceeded 26°C during the room-temperature photolysis runs.

All procedures for coirradiation were the same as above except that the furnace temperature was preset and allowed to equilibrate overnight. When a decomposition run commenced, a few minutes were required to allow the sample to reach thermal equilibrium but the light remained on and the pressure was monitored continuously.

Pressure data were recorded continuously on a Hewlett–Packard Strip Chart recorder and digitized every minute from the recorder output. Samples were encapsulated in evacuated (~10^{-3} Torr) quartz ampoules for γ-ray irradiation. The ampoules were wrapped in aluminum foil (to make them light tight) and irradiated at ambient temperatures with ^{60}Co γ rays (1.1 and 1.3 MeV) in the spent-fuel facility at Brookhaven National Laboratory. The γ-ray dose rates were 5.5 × 10^4, 1.2 × 10^6, and 5.3 × 10^6 R/hr. After gold coating the specimens were examined by an AMR scanning electron microscope with EDAX capability.

Results

The major results are in the pictures and captions contained in Plates 1–3. In order to demonstrate how the isothermal decomposition proceeds as a function of time the principal observations will be described in the order they appear with time, on pristine, unreacted material. The various decomposition stages will be described up to the final product formation with any special effects mentioned where they are encountered. Significant effects observed on the material will be included for specimens, (i) photolyzed at room temperature, (ii) coirradiated at 150°C, and (iii) preexposed to a 1.0 × 10^9-R γ-ray dose followed by photolysis. Figure 1 contains the fractional decomposi-

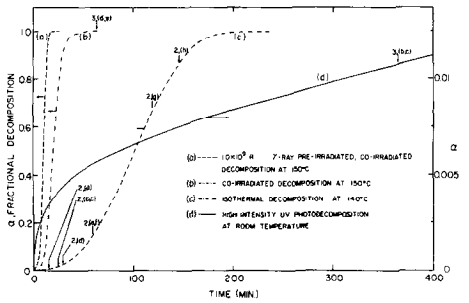

FIG. 1. Fractional decomposition, α, vs time curves for the decomposition of α-AlH_3 powder. This plot illustrates the effect of isothermal decomposition at 140°C, uv photolysis at room temperature, and coirradiation (uv photolysis and thermal decomposition) at 150°C. Also shown is the effect of exposing the material to a 1.0×10^9 R ^{60}Co γ-ray dose prior to the coirradiated decomposition at 150°C. The arrows refer to the photographs in Plates 2 and 3.

tion vs time curves for α-AlH_3 powder subjected to the various treatments and the times at which the various specimens represented in the plates were removed from the decomposition process. As a convenient reference, the arrows indicate the time and the corresponding plate number and letter.

Pristine Material

Prior to decomposition, the powder was of uniform particle size, cuboid in shape (Plate 1a), and contained several interpenetrating and contact twins of varying complexity. These cuboids appeared to be covered with a thin protective sheath of specially treated aluminum hydride (*12*), which contained deep, faceted pits and fissures in parts (Plates 1b, c). These were formed presumably during the synthesis of material. Apparently, during the synthesis and the protective-layer-formation procedure, minute traces of hydrocarbons have been incorporated into available surfaces. These carbon compounds are a possible source for the traces of CO_2 observed in the mass spectrometric analysis of the product gases. EDAX analysis of the cuboids indicated that aluminum was the only element of detectable concentration in the material.

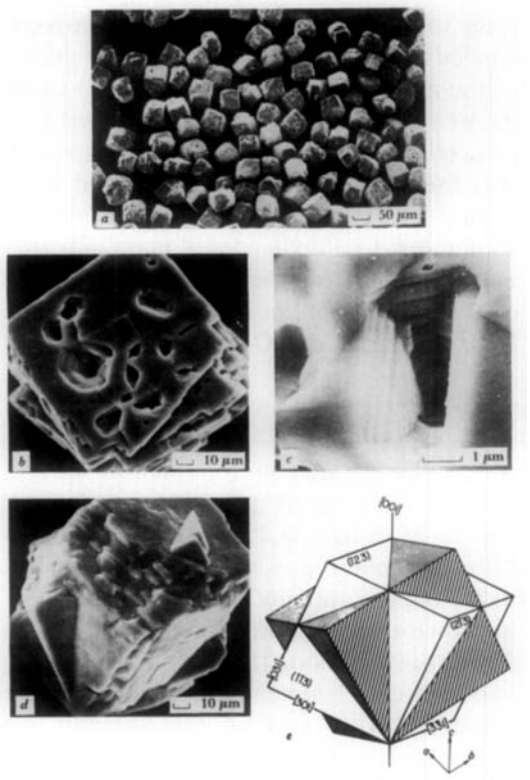

PLATE 1. Scanning electron micrographs of pristine α-AlH_3 powder. (a) Overall view of the α-AlH_3 cuboids: side lengths ~50–100 μm. Notice the variety of surface detail as well as the presence of several contact and interpenetration twinned crystals. (b) Close-up of a typical cuboid showing the presence of several surface pits. The remainder of the surface has a smooth, even appearance. The pits contain steps and layers. (c) Close-up detail of a typical surface pit showing the interior layer-like structure. Also, small sphere-like particles (0.05–0.4 μm in diameter) are shown adhering to all surfaces. (d) A simple, interpenetrating twinned cuboid crystal. Most twinned cuboids were considerably more complex than this example. (e) A drawing of an idealized penetration on twin with twin axis [001]. The twinned crystal (shaded) has been oriented to compare with (d). Also shown are the edge directions and habit faces of the cuboids determined from single-crystal X-ray analysis.

The direction of the pits' sides on the surface were determined where possible. A typical series of the more commonly occur-

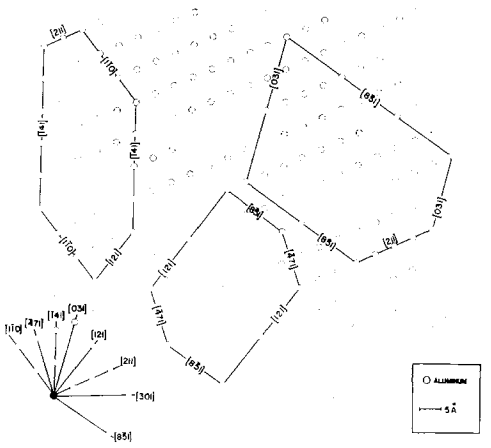

FIG. 2. The orientation of the more prominent pit edges on the $(\bar{1}\bar{1}3)$ surface of the pristine cuboids shown in Plates 1b and c. This figure also illustrates some of the other close-packed directions occurring on the surface (lower left). Occasionally surface pits are observed with edges aligned along these directions.

ring directions are shown in Fig. 2. The pits' sides are almost always aligned along one of these directions. Occasionally, more unusual directions were observed and these are also illustrated in Fig. 2 (lower left corner), where they can be seen superimposed on an aluminum atom sublattice for the $(\bar{1}\bar{1}3)$ plane which is a typical cuboid habit surface.

A layered structure was observed, Plate 1c, within the pits and fissures. These layered steps continue down to the lowest recesses of the pits and appear uniformly spaced and parallel to the upper external edge. This suggests a layered type of growth or a cyclic growth process for the formation of the cuboid. This two-dimensional layered morphology apparently is significant in the decomposition kinetics (*1*). The exposed inner layers are also covered by the protective sheath, except that it appears to be thinner on their surfaces than on the exterior.

As mentioned above, there is ample evidence of a large number of twinned crystals in the cuboids. A simple example of an interpenetration-twinned cuboid is shown in Plate 1d together with an illustration, Plate 1e, which represents the interpenetrating twin rotated to the correct angle to correspond with the photograph. The twin axis is the *c*, or [001] direction, the body diagonal of the cuboid. The twin cuboid is shaded to facilitate recognition. Also shown in Plate 1e are the [001] orientation and the surface planes which were determined from single-crystal X-ray analysis using CuK_α radiation. The [001] direction is along the cube diagonal and the habit faces are $(\bar{1}\bar{1}3)$, $(\bar{1}23)$, and $(2\bar{1}3)$, respectively.

The thermal decomposition of this material *in vacuo* at 140°C produces sigmoidally shaped, α vs time curves which have been analyzed kinetically into an induction period (a period corresponding to nuclei formation, up to $\alpha \simeq 0.1$), followed by an acceleratory period (corresponding to a nuclei growth period) and, after reaching the maximum rate, a decay period (corresponding to a stage involving a contracting reactant/product interface). The following paragraphs will describe the SEM observations occurring during these periods, in sequence.

Rough surface patches are observed occasionally during the induction period (Plate 2a). These patches appear to be sparsely scattered over the surface and on the sides of the interior of the pits and fissures (Plate 2b). This indicative of surface layer subsidence to expose the reacted area beneath. The subsidence could arise from subsurface contraction of the reaction product interface as the product forms and collapses. These patches were found in increasing number during the induction period (up to 25 min at 140°C). The patches contain finely divided acicular filaments of aluminum metal (Plate 2c). Apparently, subsurface decomposition generates these filaments and they become visible where areas of the subsurface are exposed. At this

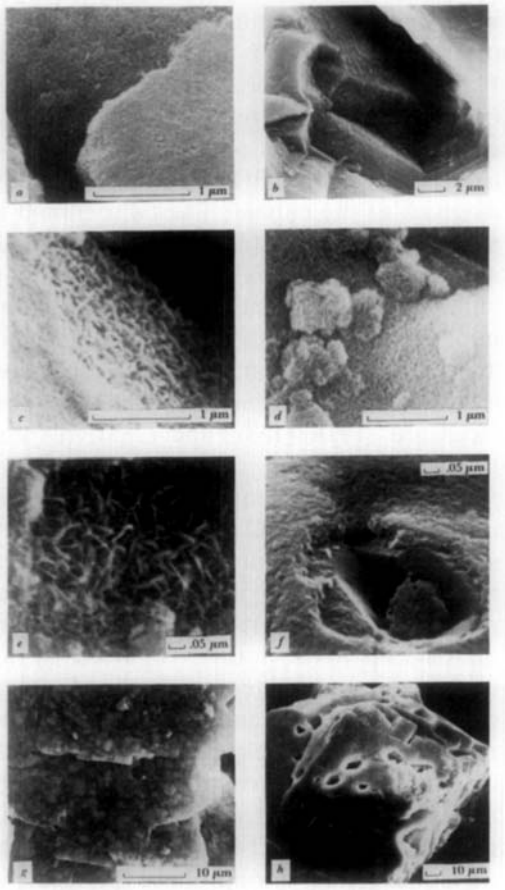

PLATE 2. Scanning electron micrographs of α-AlH_3 powder during various stages of thermal decomposition at 140°C *in vacuo*. (a) 15 min (during the induction period)—close-up of a rough, surface patch showing the fine structure consisting of acicular filaments approximately 0.1 μm in length. These are present in some regions of the cuboids prior to decomposition where they appear to be even smaller in size. (b) 25 min (end of induction period)—close-up of a surface pit showing two small patches of fine filamentary crystals (upper center). These regions containing acicular crystals are also found in cracks and fissures originating at the surface. (c) 25 min—close-up detail of upper patch in (b) above. Note the cylindrical nature of the filaments and their separateness. Apparently they form randomly below the surface and grow preferentially along one direction (possibly the [001]). They appear to have collapsed into a mixed heap within the patch. (d) 30 min—close up of small irregularly shaped particles (0.3–0.9 μm across) adhering to surface. These appear to be clusters of aggregated acicular crystals. (e) 60 min—maximum magnification of filaments. An EDAX scan of this material indicates only the presence of aluminum. (f) 60 min—collapse of a local surface region showing decomposed material underneath the protective surface. (g) 120 min—gas bubbles visible just beneath surface. These bubbles vary in size from 0.2 to 3.5 μm (at this stage of the decomposition) and appear uniformly scattered throughout the crystal. (h) 145 min—degradation of cuboid edges and corners. This does not differ significantly from samples examined at times greater than 145 minutes, i.e., the degradation appears to be caused by the collapse of the internal substructure and probably by removal of the bubbles and is not directly related to the decomposition time sequence.

stage the filaments are elongated ellipsoids, ~0.005 μm in diameter and 0.1 μm in length, and are dispersed in a random manner within the subsurface patch. At the patch/unreacted-solid interface the filaments appear to decrease in size toward the interior of the crystal but a sharp interface was *not* observed (within the resolution of the microscope). The filaments continue to decrease in size toward the unreacted matrix. Also it is important to note that the filaments can be found dispersed occasionally in some parts of unreacted, pristine material. As will be shown from both the kinetic studies (*1*) and the uv photolysis experiments reported below, exposure to uv light will induce decomposition. Presumably these areas in the pristine material have aged (decomposed) on prolonged storage; the presence of the filament nuclei suggests that the aging process is probably a slow photolysis. During thermal decomposition these patches were usually not found on the protected external surface or even at the intersection of the penetrating twin faces but frequently are in the inner surfaces of the pits and fissures. The protected external surface remains as a "cocoon" throughout the entire decomposition process and very rarely shows evidence of decomposition, though it does fracture occasionally toward the end of the reaction. This permits the cuboid to retain its overall

shape even as the filamentary decomposition process continues internally.

As the isothermal decomposition process enters the acceleratory period (Plate 2d), small clusters of aggregated lumps of filaments appear on the reacted surfaces. These aggregatres are approximately spherical in shape and appear to adhere to the surface where the filaments are found. Plate 2e shows a typical aggregate lying inside a naturally occurring hole in a surface. The reason for the formation of these clusters has not been determined; possibly they are lumps of partially reacted or oxygen-coated material which have loosened and fallen away from the surface. EDAX scans of these areas indicate that aluminum is the only detectable metal present in the aggregate.

After heating for 60 min, the filaments themselves appear to thicken and increase in length (Plate 2e). It would appear that, in addition to their formation in the decomposition process, some mechanism exists for these filaments to grow slightly in size. It has not been determined whether they grow within the patch or are formed in the host material, grow and ultimately collapse into the patch. However, the number of filaments (and patches) increases markedly as the reaction proceeds. These patches are randomly distributed throughout the crystal and contain varying sizes of filaments. As the reaction continues in the acceleratory period, large gas bubbles (voids) appear in the cuboid. Plate 2g shows evidence of these bubbles located just below the surface after heating for 120 min. These bubbles vary in diameter from 0.2 to 3.5 μm and appear uniformly distributed throughout the cuboid. Eventually the internal substructure collapses in parts, leaving a finely divided filamentary cuboid with an almost continuous shell. Degradation of the cuboid edges and corners are evident (Plate 2h), possibly due to the collapse of the internal substructure, and the removal of the bubbles. This morphology does not differ significantly from that of samples examined at longer decomposition times. Within the completely reacted cuboid, subparticles remain consisting of aggregated filamentary blocks or volumes ranging in diameter from 0.2 to 3.5 μm.

The effects induced by subjecting this material to various pretreatments are illustrated in Plate 3. These include the effects of exposure to a 1.0×10^9-R dose of ^{60}Co γ-rays, material uv photolysed at room temperature, and the effects of simultaneous thermal and uv decomposition at 150°C.

The material is blackened by ^{60}Co γ-ray doses above 1.0×10^8 R. This blackening appears to have little effect on the SEM pictures which closely resemble those for the pristine material. However, the immediate external surface does appear to be much rougher and contains a few patches of the filaments. It is proposed that the blackening of the surface is associated with the formation of the surface "roughness" of finely divided intermeshed filaments—which has the appearance of a finely divided metal (black). The decomposition process at 150°C is markedly accelerated by the presence of these additional small filaments (see Fig. 1a). However, the decomposition sequences do not differ significantly from those observed in pristine material except that more filaments are present and each stage occurs more rapidly.

After uv photolysis at room temperature into the linear rate region (Fig. 1d) the surface of the cuboids appears to be silver colored. Again, surface patches are visible and these contain multitudes of fine filaments, approximately 0.03 μm in diameter. These are similar to the thermal decomposition product (Plate 3b). Also the surface contains several regions in which the needles appear to have formed aggregates (Plate 3c). The silvery appearance of the photolysed surface may be due to denser

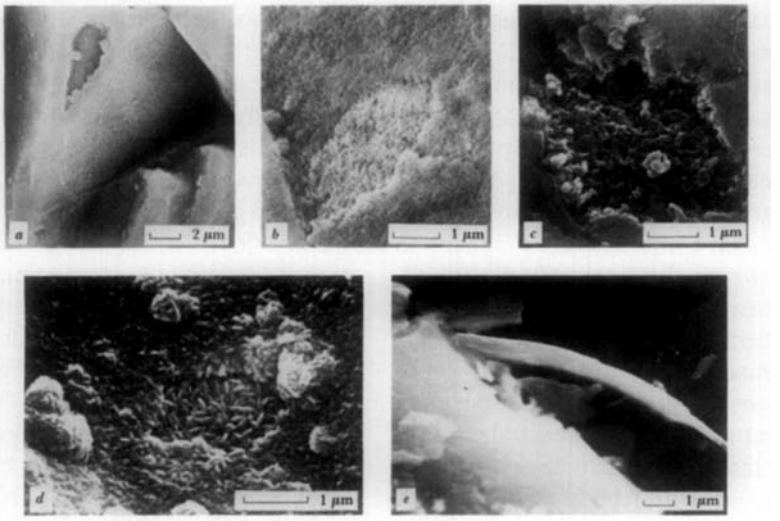

PLATE 3. Scanning electron micrographs of 1.0×10^9 R ^{60}Co γ-ray irradiated, uv photolyzed and uv coirradiated at 150°C, α-AlH_3 powder samples. (a) 1.0×10^9 R ^{60}Co γ-ray irradiated—The surface appears black under room light and SEM revealed a generally rougher surface. This picture illustrates a typical surface patch formed after irradiation prior to thermal decomposition. (b) uv photolysis—370 min of exposure to intense uv light *in vacuo* at room temperature. The cuboids appear silvery under room light. A close-up of a surface patch showing a multitude of fine needles (similar to the thermal decomposition product) is pictured here. This strongly suggests that the acicular crystals are formed as a result of decomposition and probably are the decomposition nuclei. (c) Same conditions as (b)—an example of another surface patch showing a considerably rougher texture. This region may have formed by aggregation of the needles. (d) 60 min of uv coirradiated decomposition at 150°C ($I = 67$ mW cm^{-2})—Note the coarser structure of the product nuclei. This may be due to a synergistic uv–thermal effect. (e) Same conditions as (d)—an instance of surface delamination indicating the lack of cohesiveness of the surface layer as the decomposition proeeds and its imperviousness during decomposition.

patches of metal nuclei. One additional effect which is observed in the coirradiated crystals is that the protective surface layer delaminates in some sections (Plate 3e). This indicates that, as the subsurface reaction proceeds, a lack of cohesiveness results between the surface layer and the decomposition product. It is also an indication of the imperviousness of this layer throughout the entire decomposition.

Simultaneous thermal and photolytic decomposition at 150°C produced surface patches that have given the clearest picture to date of the needle-like substructure within a patch (Plate 3d). The filaments appear to be thicker (diameter ~0.05 μm) than at the beginning of the reaction (diameter ~0.005–0.02 μm). However, it was not possible to attribute this additional increase in thickness solely to the coirradiation effect. Also it would appear that, at this magnification (~× 15,000), the sides of some of the needles appear faceted, but details are not resolvable.

Discussion

The observations described above on the pristine and thermally and uv-decomposed α-AlH_3 are relevant to the respective decomposition kinetic studies. These observations can be grouped into three categories; viz., pristine material, thermally decomposed material, and material sub-

jected to various irradiations. For pristine material, the significance of the outer coating is obvious. It is impervious to air and water vapor and, to a large degree, to ambient thermal effects. Aging similar to partial exposure to light has occurred over several years of storage and has induced areas of decomposition in the material as indicated by the presence of the acicular filaments in some regions prior to decomposition. (Also the material is gray in color; on synthesis, it was reported to be white (*11*)). Furthermore, the presence of the large number of twinned crystals may be explained by examining the $R\bar{3}c$ trigonal space-group packing of the unit cell. An infinite number of interpenetration cube twins can be obtained with the [001] direction as a twin axis. Also the columns and rotating spirals of the Al and H atoms in the unit cell easily lend themselves to contact twin formation and, on an atomic scale, to a columnar-type nucleus. Interestingly, evidence could not be found for increased reactivity at the intersection of twin boundaries. The interior layered structure is of great significance in defining the progress of the thermal reaction through the solid. These photographs of the layered structure supply supportive evidence for the kinetic analysis presently underway (*1*). These results will be reported elsewhere. The presence of the outer layer seems to do little to hinder the thermal decomposition process from occurring. The unit cell packing clearly shows the Al and H atom layers and the growth of the crystal along these directions is not unexpected. The edges of the surface pits generally lie along close-packed directions as is expected by their growth during synthesis. It seems reasonable that these directions should be important in the propagation of the reaction into the solid. The uniformity of the particle size of the powder and of the acicular needles underlies the reason why reproducibility of these effects is so consistently excellent.

The acicular needles of aluminum are considered to be the product nuclei formed in the thermal decomposition process. From the present observations it appears that the needles are formed randomly, in large numbers, early in the decomposition, probably via a process closely resembling the formation of a latent image in the silver halides (*13*). These initial nuclei are likely to be colloidal in dimensions as proposed by Pimenov (*14*) and their subsequent growth depends on the topochemical nature of their surroundings. Their final shape suggests that one direction (possibly the [001] as suggested by Mikhailov *et al.* (*7*) dominates in the growth process. At least two growth models can be proposed to account for the final shape: (1) that unidirectional growth dominates throughout the whole growth process, or (2) that the unidirectional growth is extremely rapid and then is terminated (for example, as can occur by growth between two layers) and the slower growing directions then proceed to thicken the needles as the reaction continues. This latter growth mechanism is favored by the present observations. Presumably the large number of nuclei prevents them from growing very large.

The aggregates of needles and partially reacted lumps can be attributed to reactant spalling off from regions on the surface as the reaction proceeds into the crystal interior. These clusters appear on all the surfaces and are of varying sizes and shapes (mostly spherical).

The presence of the bubbles (probably containing hydrogen gas) in the later stages of the decomposition, serves to break up the crystal into smaller aggregated blocks. This supports kinetic analysis evidence of a contracting interface mechanism operating in some type of (isolated) crystal volume.

Enhancement of the thermal decomposition kinetics by preexposure of the sample to γ-ray doses up to 1.0×10^9-R seems reasonably accounted for by the presence

of the multitude of additional filaments present in the sample after a 1.0×10^9-R irradiation prior to decomposition. These nuclei have been formed by the irradiation and are present at $t = 0$. At lower doses it has been shown kinetically (*1*) that the number or "size" of nuclei during the induction period is a linear function of log Φ. (Φ = the γ-ray dose.) The blackening of the material (and presumably the surface coverage by the filaments) does increase as the dose increases up to 1.0×10^9 R.

Photolysis with uv light induces the same type of decomposition as the thermal process except the decomposition appears to be confined to areas just below the surface. Also, the filaments tend to aggregate into a more condensed type of substructure. This condensation or aggregation of the needles may be due to the thermal effects of the light on layers close to the surface. This is a possible explanation for the absence of an induction (and acceleratory) period in the photodecomposition curves at room temperature. The number of nuclei formed instantly in the surface layers is so large (because of the lamp intensity) that nuclei growth is minimal. At lower lamp intensities at room temperature the experimental curves do contain a slight acceleratory period (*1*). The effects of simultaneous uv and thermal decomposition are similar to the effects already described except the needle-like nuclei appear to be slightly thicker and larger. In all cases the sites for formation of these nuclei are randomly distributed. However, the observations are confined to layers on the exposed surfaces or within the collapsed protective sheath. Grinding of the powder showed little evidence for the method of propagation of the reaction within the solid except that the particles all contain acicular filaments. The crystals do not cleave but exhibited signs of conchoidal fracture. It is likely that the growth of these filaments or patches containing them will also occur in layers (as the growth of the crystal seems to have followed a similar route). Solid state defects and electron carriers are likely to be involved in the energy transfer mechanisms induced by the radiation.

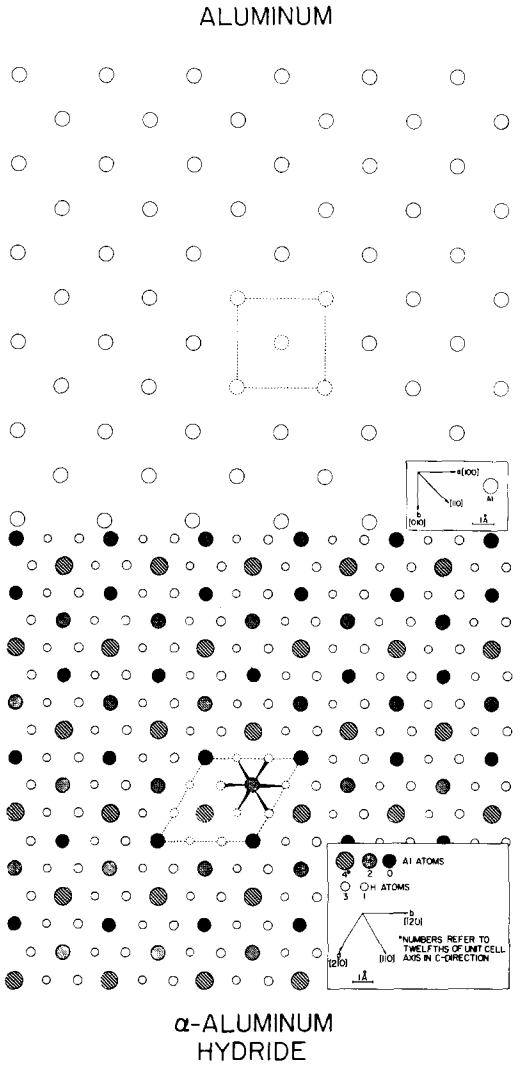

FIG. 3. A comparison of the lattice spacing of the *c*, (001), face of Al metal and the *c*, (001), face of α-AlH_3. Notice, in particular, the increased separation between the Al atoms in the α-AlH_3 lattice at the interface. This suggests that during decomposition, the α-AlH_3 lattice has to shrink to accommodate the Al-metal product. Presumably, this shrinkage would induce stress at the product/reaction interface.

The formation of aluminum metal in a host aluminum hydride lattice obviously involves contraction along an interface. This is illustrated in Fig. 3 which shows the lattice spacings between aluminum atoms in the c, (001), face of aluminum metal and a c, (001), face of α-AlH_3. As can be clearly seen, the interatomic distance between atoms in the metal is less than in the hydride. This would indicate that some type of contraction occurs at the reactant/product interface. This contraction could be such as to curve the interface and allow the needles to form and "peel off" or spall-off as ellipsoids. The strain at the interface would assist propagation of the reaction, if dislocations, point defects, voids, etc., were formed ahead of the interface into the reactant. This strain may assist the formation of the bubbles present in the solid at the late stages of the decomposition. This study clearly indicates that the decomposition of α-AlH_3 is similar to the many heterogeneous nucleation and growth decomposition studies previously reported (*14*). These studies suggest that in addition to dislocations and the solid-state defects, electronic carriers and/or a charge-transfer-type mechanism may be operative in the decomposition. The role of these carriers in the decomposition of α-AlH_3 is currently being investigated and will be reported elsewhere.

References

1. P. J. HERLEY AND O. CHRISTOFFERSON, *J. Phys. Chem,* in press (1981).
2. P. J. HERLEY AND R. H. IRWIN, *J. Phys. Chem. Solids* **39,** 1013 (1978).
3. P. J. HERLEY, P. W. M. JACOBS, AND P. W. LEVY, *Proc. Roy. Soc. (London), Sec. A* **318,** 197 (1970).
4. P. W. M. JACOBS AND F. C. TOMPKINS, *in* "Chemistry of the Solid State" (W. E. Garner, Ed.), Chap. VII, Butterworth, London (1955).
5. D. A. YOUNG, "Decomposition of Solids," Pergamon, London (1966).
6. F. C. TOMPKINS, *in* "Solid State Chemistry" (N. B. Hannay, Ed.), Vol. 4, p. 193, Plenum, New York (1976).
7. YU. I. MIKHAILOV, YU. G. GALITSYN, AND V. V. BOLDYREV, *Kinet. Catal. (USSR)* **17,** 608 (1976).
8. J. W. TURLEY AND H. W. RINN, *Inorg. Chem.* **8,** 18 (1969).
9. G. C. SINKE, L. C. WALKER, F. L. OETTING, AND D. R. STULL, *J. Chem. Phys.* **47,** 2759 (1967).
10. P. J. HERLEY AND P. W. LEVY, *J. Chem. Phys.* **46,** 627 (1967).
11. F. M. BROWER, N. E. MATZEK, P. F. REIGLER, H. W. RINN, C. B. ROBERTS, D. L. SCHMIDT, J. A. SNOVER, AND K. TERADA, *J. Amer. Chem. Soc.* **98,** 2450 (1976).
12. N. E. MATZEK, Dow Chemical Co., U.S. Patent 3,844,854 (1974).
13. J. W. MITCHEL, "Chemistry of the Solid State" (W. E. Garner, Ed.), Chap. XIII, Butterworth, London (1955).
14. YU. D. Pimenov, *Opt. Spectrosc. (USSR)* **43,** 53 (1977).
15. For example, see J. M. THOMAS AND J. O. WILLIAMS, *in* "Surface and Defect Properties of Solids" (M. W. Roberts and J. M. Thomas, Eds.), Chem. Soc. Spec. Pub. Vol. 1, p. 1, Chem. Soc., London (1972).